Nuclear Inst. and Methods in Physics Research, A 871 (2017) 97–104

Contents lists available at ScienceDirect

Nuclear Inst. and Methods in Physics Research, A

journal homepage: www.elsevier.com/locate/nima

Charge production studies from Cs_2Te photocathodes in a normal conducting RF gun

C. Hernandez-Garcia *[,1], M. Krasilnikov, G. Asova [2], M. Bakr [3], P. Boonpornprasert, J. Good, M. Gross, H. Huck, I. Isaev, D. Kalantaryan, M. Khojoyan [4], G. Kourkafas [5], O. Lishilin, D. Malyutin [5], D. Melkumyan, A. Oppelt, M. Otevrel [6], G. Pathak, Y. Renier, T. Rublack, F. Stephan, G. Vashchenko [7], Q. Zhao [8]

Deutsches Elektronen Synchrotron DESY, Platanenallee 6, 15738 Zeuthen, Germany

ARTICLE INFO

Keywords:
RF electron guns
Space charge
Laser radial halo

ABSTRACT

This work discusses the behavior of electron bunch charge produced in an L-band normal conducting radio frequency gun from Cs_2Te photocathodes illuminated with ps-long UV laser pulses and presumed homogeneous flattop laser transverse distribution. The measured charge shows the expected linear dependence in the quantum efficiency limited emission regime at low laser pulse energies. At higher laser pulse energy, the measured charge in the space charge limited emission regime should saturate, assuming an ideal homogeneous flattop laser transverse distribution. However, this behavior is not observed experimentally. Instead of saturating, the measured charge continues to increase with laser pulse energy, albeit with much weaker dependence than in the quantum efficiency limited emission regime. Simulations with the space charge particle tracking code ASTRA show that the charge saturates as expected using a homogeneous flattop laser transverse distribution. The discrepancy between simulations and measured excess charge may be attributed to the presence of unintentional Gaussian-like decaying radial halo beyond the core of the otherwise presumed homogeneous flattop core. The rate of increase of the measured charge at high laser pulse energies seems to be proportional to the amount of halo despite charge saturation in the core of the transverse laser radial profile. By utilizing core + halo particle distributions based on measured radial laser profiles, ASTRA simulations and semi-analytical emission models reproduce the behavior of the measured charge for a wide range of RF gun and laser operational parameters within the measurement uncertainties.

Published by Elsevier B.V.

1. Introduction

The Photo Injector Test facility at DESY, Zeuthen site (PITZ) [1], is dedicated to the development and optimization of high-brightness electron sources for free-electron lasers (FELs), such as FLASH [2], and the European XFEL in Hamburg that require nanocoulomb (nC) electron bunches of 10–20 ps in length with extremely small transverse emittance [3]. In order to compromise between intrinsic cathode (thermal) and space charge induced emittance, production of electron bunches with high phase space charge density leads to electron emission near the space charge (SC) limit. This imposes stringent operational settings on the photoinjector such as accelerating radio frequency (RF) fields in

* Corresponding author. Fax: +1 (757) 269 5199.
E-mail address: chgarcia@jlab.org (C. Hernandez-Garcia).
[1] On leave from Jefferson Lab, 600 Kelvin Dr. Ste. 8, Newport News, VA 23606, USA.
[2] On leave from BAS INRNE, 1784 Sofia, Bulgaria.
[3] On leave from Assiut University, 71515 Assiut, Egypt.
[4] Now at Synchrotron SOLEIL, Paris, France.
[5] Now at Helmholtz-Zentrum Berlin, Berlin, Germany.
[6] Now at the Central European Institute of Technology, Brno, Czech Republic.
[7] Now at DESY, Hamburg, Germany.
[8] On leave from IMP/CAS, 730000 Lanzhou, China.

http://dx.doi.org/10.1016/j.nima.2017.06.051
Received 3 March 2017; Received in revised form 15 June 2017; Accepted 28 June 2017
Available online 18 July 2017
0168-9002/Published by Elsevier B.V.

the order of tens of mega volts per meter and very stable generation of space charge dominated electron bunches.

The PITZ photoinjector consists of a 1.6 cell L-band normal conducting radio frequency (RF) gun with a main-bucking focusing solenoid pair and a Cs_2Te photocathode, a normal conducting RF booster cavity, a transport line with electron beam diagnostics, and a photocathode UV laser system with associated beam transport and diagnostics. By means of a temporal pulse shaper, the laser system can be tuned to generate from short (~2 ps FWHM) Gaussian pulses to long (~20 ps FWHM) flattop pulses, allowing the RF gun to produce bunch charges up to a few nC at maximum momentum of 7 MeV/c. The photoinjector optimization in 2008–2009 for bunch charges of 1, 0.5, 0.25, and 0.1 nC resulted in measured emittance values which met the requirements of the European XFEL [4]. With further improvements of the PITZ photoinjector in 2010–2012 even smaller emittance values were achieved, albeit a rather large discrepancy was observed between measured and simulated projected transverse emittance as a function of laser rms spot size on the cathode as described in Ref. [5]. The optimum laser spot size on the cathode corresponding to the minimum projected transverse emittance measurements is smaller compared to that predicted by ASTRA beam dynamics simulations [6] assuming an ideal homogeneous flattop laser transverse distribution [5]. The discrepancy in optimum laser spot size is almost negligible for bunch charges below 0.1 nC, but becomes larger with increasing bunch charge.

Although the transverse phase space is one of the critical electron beam quality benchmarks demonstrated at PITZ for the European XFEL, this is a higher order beam dynamics effect compared to bunch charge production. Bunch charge measurements as a function of laser pulse energy for the short Gaussian and for the long flattop temporal laser pulses consistently show that the bunch charge continues to increase asymptotically in the space charge limited emission regime for a wide range of RF gun parameters. In contrast to these experimental measurements, ASTRA simulations show that the charge saturates as expected when an ideal input particle distribution consisting of a flattop radial profile is used in conjunction with experimental temporal laser and RF gun parameters. This work focuses on studying the sources for this discrepancy. Observations of the actual transverse laser distribution illuminating the photocathode indicate the presence of halo extending beyond the flattop core intended to be generated with the laser beam transport system. Therefore, unintended halo in the laser radial profile may contribute to the measured additional bunch charge, but this is not observed in the simulations as long the ideal flattop laser transverse distribution is utilized.

2. Experimental setup and procedures

The photocathode laser system provides UV pulses with a wavelength of 257 nm and a maximum energy of ~10 μJ per micropulse by means of an Yb:YAG regenerative amplifier and a two-stage Yb:YAG booster amplifier in combination with frequency conversion crystals [1,2,7]. The system is capable of generating pulse trains containing up to 800 micro-pulses separated by 1 μs at 10 Hz repetition rate. The laser pulse energy delivered to the photocathode can be adjusted remotely via a rotatable half-wave plate followed by a birefringent crystal used as a polarizer. A pick-off mirror (3.6% reflectivity) directs a fraction of the laser beam to an energy meter. The actual laser pulse energy on the photocathode is calculated from this measurement taking into account ~91% transmission of the vacuum window, and ~85% reflectivity of the vacuum mirror.

2.1. Temporal profile of the laser pulses

The temporal shaping of the micro-pulses takes place in the laser room, before the laser beam line (LBL) that transports the beam to the photocathode RF gun in the accelerator tunnel. The flexibility of the laser system allows production of Gaussian pulses in a variety of lengths, from ~2 ps FWHM with no manipulation, up to ~11 ps FWHM with a Lyot filter in the regenerative amplifier. In addition, the Gaussian pulses can be transformed into a temporal flattop profile with rise and fall times as short as ~2 ps and pulse lengths between 17 and 24 ps FWHM by means of a longitudinal pulse shaper based on 13 birefringent crystals [7]. The temporal profile of the UV output pulses was characterized with an optical sampling system (OSS) based on an optical cross-correlation technique with resolution better than 1 ps [7]. Fig. 1 shows an example of these measurements.

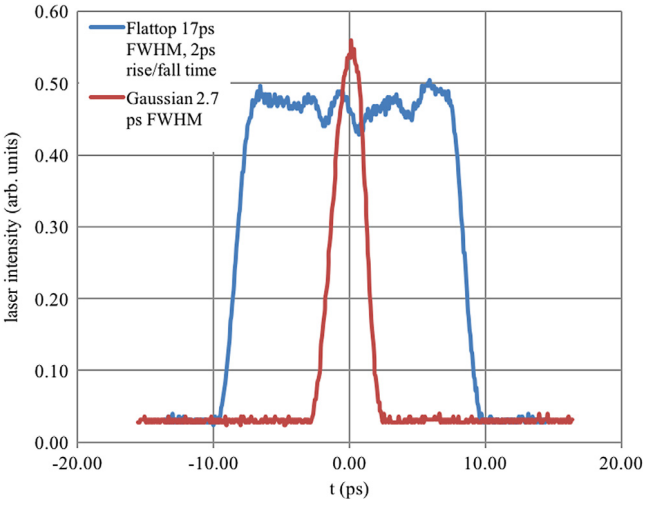

Fig. 1. Laser temporal profiles measured with the OSS.

2.2. Transverse profile of the laser pulses

The transverse shaping of the UV laser pulses is performed in the LBL [1]. The laser spot at the conversion crystals is imaged onto a Beam Shaping Aperture (BSA). The BSA is imaged through a vacuum window and reflected off a vacuum mirror at nearly normal incidence onto the RF gun photocathode for producing a homogeneous radial distribution. The diameter of the BSA can be finely adjusted with a remotely controlled iris diaphragm, while its position relative to the laser beam path can be set also remotely via stepper motors. Remote controllable mirrors allow positioning of the laser spot on the photocathode, thereby aligning the laser spot center with the electrical axis of the gun cavity. The photocathode laser transverse distribution characterization is detailed in Appendix.

2.3. Charge measurements as a function of laser pulse energy

The experiments consisted in measuring bunch charge as a function of laser pulse energy. The charge was measured with a Faraday cup located ~0.8 m downstream of the photocathode. The cathode accelerating RF field is given by

$$E_{cath} = E_0 \sin(\varphi) \tag{1}$$

where $\varphi = \Phi_0 - \Psi$, E_0 is the peak longitudinal component (accelerating) of the electric RF field, Φ_0 is the zero-crossing phase and Ψ is the gun set-point (SP) phase. Practically, the phase offset Φ_0 is a parameter determined within the Low Level RF system and thus is dependent on its setup, e.g. on the peak RF power in the gun as well as resonance conditions of the cavity. The nominal operation phase of the RF gun is set for the Maximum Mean Momentum Gain (MMMG) of electron beam. The MMMG phase is determined by measuring the beam momentum as a function of gun phase using a 60° bending dipole spectrometer located between the RF gun and the booster cavity [4]. Because of the flatness of

Table 1
Laser and RF gun parameters utilized for each experimental setup. For setups 1–4 the indicated RF gun phase corresponds to the Maximum Mean Momentum Gain (MMMG). E_{cath} is calculated using Eq. (1). The laser pulse length was measured with the Optical Sampling System for setups 1–4, while an extrapolation of earlier measurements with YLF Lyot filters (6 mm–4 ps FWHM, and 16 mm–7 ps FWHM) would suggest a FWHM pulse length of ~3.5ps FWHM [7,8] for setups 5–7. For setups 8–10 there was no Lyot filter in the laser regenerative amplifier; therefore, the Gaussian laser pulse is estimated to be about 2 ps FHWM.

Setup	BSA diameter (mm)	Laser temporal profile	Laser pulse length FWHM (ps)	Gun RF power (MW)	Gun RF Phase (deg)	E_0 (MV/m)	E_{cath} at moment of emission (MV/m)
1	1.2	Gaussian	2.7	4.0	39	45.9	29.0
2	1.2	Gaussian	2.7	7.75	46	62.7	45.0
3	1.2	Flattop	17.0	4.0	39	45.9	29.0
4	1.2	Flattop	17.0	7.75	46	62.7	45.0
5	0.8	Gaussian	3.5	1.5	90	29.0	29.0
6	0.8	Gaussian	3.5	3.375	90	43.5	43.5
7	0.8	Gaussian	3.5	6.0	90	58.0	58.0
8	0.8	Gaussian	2.0	6.0	90	58.0	58.0
9	0.8	Gaussian	2.0	6.0	49	58.0	43.5
10	0.8	Gaussian	2.0	6.0	30	58.0	29.0

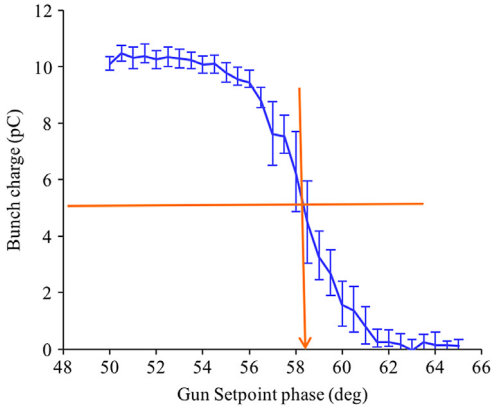

Fig. 2. Typical phase scan for determining the zero-crossing phase Φ_0, indicated by the arrow, corresponding to the phase for which the charge is $\frac{1}{2}$ of the maximum as indicated by the arrow.

the mean momentum dependence on the gun phase, the reference phase determination has a resolution of ~0.5°–1.0°. The zero-crossing phase was estimated by setting the bunch charge to about 10 pC (significantly below space charge limited emission for the nominal operation phases) and measuring the charge as a function of gun phase until the charge saturated due to the quantum efficiency limited emission [1]. The gun phase that corresponds to the point where the extracted charge is $\frac{1}{2}$ of the saturated charge value is the zero-crossing phase, as shown by the phase scan in Fig. 2. The uncertainty in the estimation depends on the effect of the image charge on the phase scan and on phase jitter (laser pulse arrival time with respect to the gun RF launch phase). Table 1 indicates the parameter space for each experimental setup.

3. Results and discussion

3.1. Semi-analytical analysis of the effect of halo on measured charge

The laser spot size on the cathode for setups 1–4 was established using the BSA set to 1.2 mm for both types of temporal pulses. The laser diode pumps were readjusted during tuning of the laser temporal profile. As a result, a larger laser energy range was applied for the case of the flattop profile. This can explain a difference in the overall intensity between both distributions shown in Fig. 3. Note that the measured rms transverse size is 0.312 mm compared to 0.30 mm expected from an ideal flattop core radial profile with 1.2 mm diameter. The laser transverse distributions in Fig. 3 suggest the presence of halo (dark blue) extending beyond the core (green), which in addition exhibits intensity variations (red hot spots) in a ring-like fashion. This is due in part to diffraction effects leading to radial modulations and deviation from the designed radial flattop shape. Several optical elements (several lenses and mirrors, and a beam splitter) were placed in the vicinity of the Fourier plane of the BSA-to-photocathode laser beam imaging system. Additionally, their apertures (5 cm diameter) truncate high frequency spatial harmonics. These perturbations are most pronounced for smaller spot sizes when the image in the Fourier plane has rather large dimensions (see Appendix). Such laser radial profile can be represented to a first approximation by a homogeneous core distribution (without considering the intensity fluctuations within the center part) and a decaying halo outside the core with the following equation

$$F(r) = \frac{E_l}{\pi R_c^2 + 2\pi\xi\sigma_r^2} \begin{cases} 1, & r \le R_c \\ \xi \cdot e^{\left(\frac{R_c^2 - r^2}{2\sigma_r^2}\right)}, & r > R_c \end{cases} \tag{2}$$

where $E_l = 2\pi \int_0^\infty F(r)\, r dr$ is the laser pulse energy, R_c is the radius of the core, ξ is the relative intensity of the Gaussian halo with respect to the intensity of the core, and σ_r is the rms size of the Gaussian halo profile.

The charge measurements vs. laser pulse energy for setups 1–4 shown in Fig. 4 were taken with RF gun power settings of 4.0 W (E_0 = 45.9 MV/m) and 7.75 MW (E_0 = 62.7 MV/m) at the MMMG gun phase. Measured momentum distributions at the MMMG phase for these power settings have center of mass at 5.32 MeV/c and 7.09 MeV/c correspondingly. Beam dynamics simulations yield cathode accelerating fields at the moment of emission of 29 and 45 MV/m, respectively. For setups 1 and 2 the estimated rms phase jitter was ~2.5°, whereas for setups 3 and 4 the rms jitter was ~1.8°.

In the space charge (SC) limited emission regime (high laser pulse energy, Fig. 4) the measured charge vs. laser pulse energy for setup 1 shows the strongest saturation, while for setup 4 shows the most linear behavior of the measurements. In the quantum efficiency (QE) limited emission regime (lower laser pulse energy) the behavior for setups 1–4 is linear as expected.

The surface space charge density assuming a radially homogeneous core with Gaussian-like decaying halo can be described by

$$\sigma'_Q(r) = \frac{2 \cdot QE \cdot E_l}{\pi R_c^2 + 2\pi\xi\sigma_r^2} \begin{cases} 1, & r \le R_c \\ \xi \cdot e^{\left(\frac{R_c^2 - r^2}{2\sigma_r^2}\right)}, & r > R_c \end{cases} \tag{3}$$

where the approximate factor *2* comes from the calculation of the QE given in % $QE = \frac{hc}{e\lambda} \cdot \frac{Q}{E_l}$ for λ = 257 nm, and considering that E_l is given in nJ and the bunch charge Q in pC. A simple model to estimate the effect of halo contributing to extracted charge beyond saturation in the core can be applied to our laser radial profile [9]. By taking into account the space charge density limit $\sigma_{scl} \propto E_0 \sin\varphi_0$ [5] and denoting $Q_{max} = \sigma_{scl} \cdot \left(\pi R_c^2 + 2\pi\xi\sigma_r^2\right)$ as the limiting charge value, assuming a space charge limitation the produced charge can be calculated as:

$$Q = Q_{core} + Q_{halo}, \tag{4}$$

where the charge in the core is given by:

$$Q_{core} = \frac{1}{1+\xi\eta} \begin{cases} Q_{th}, & \text{if } Q_{th} \le Q_{max} \\ Q_{max}, & \text{if } Q_{th} > Q_{max}. \end{cases} \tag{5}$$

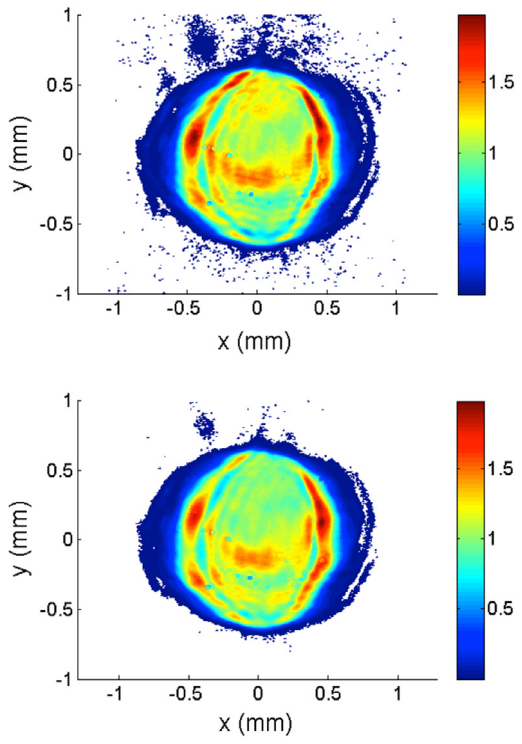

Fig. 3. Laser transverse distribution images for BSA = 1.2 mm captured with a UV-sensitive CCD camera placed at a location optically equivalent to the real cathode position for the flattop temporal profile (top) with measured $\sigma_{xy} = 0.313$ mm and for the Gaussian temporal profile (bottom) with measured $\sigma_{xy} = 0.312$ mm. (For interpretation of the references to color in this figure legend, the reader is referred to the web version of this article.)

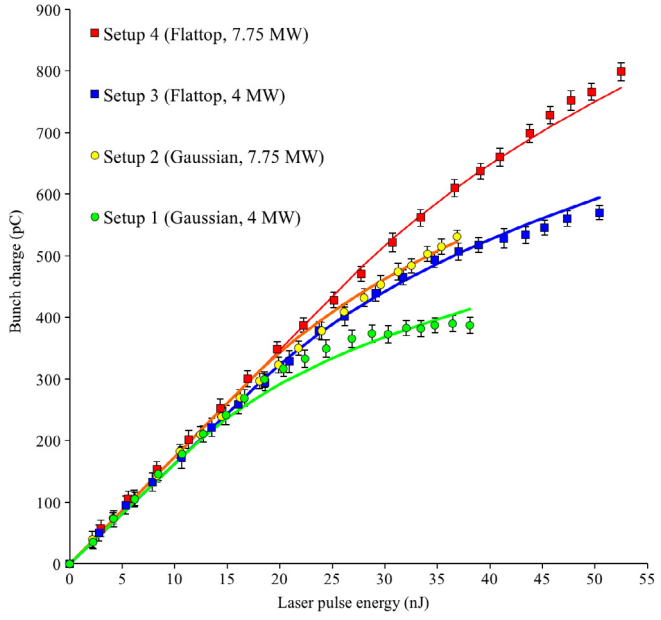

Fig. 4. Measured charge vs. laser pulse energy for setups 1–4. The solid lines show the results of the semi-analytical model (Eqs. (2)–(6)) applied to the corresponding measurements.

The charge in the halo can be calculated as:

$$Q_{halo} = \frac{\eta}{1+\xi\eta}\begin{cases}\xi Q_{th}, & \text{if } \xi Q_{th} \le Q_{max}\\ Q_{max}\cdot\left(1+\ln\frac{\xi Q_{th}}{Q_{max}}\right), & \text{if } \xi Q_{th} > Q_{max}\end{cases} \quad (6)$$

Table 2
Fit parameters for the model (2)–(6) with $\xi = 0.98$, and $\eta = 1.17$ for flattop (17 ps FWHM) and for Gaussian (2.7 ps FWHM).

Laser temporal profile	RF peak power (MW)	QE (%)	Q_{max} (pC)
Flattop	7.75	8.36	673
Gaussian			445
Flattop	4.00	8.01	432
Gaussian			285

where Q_{th} given in pC is the theoretically expected emitted charge in the QE limited emission regime, and $\eta = 2\sigma_r^2/R_c^2$ for the halo-core rms area ratio. From the dimensionless squared halo-core ratio $\eta = 1.17$ found from the curve fit, and assuming that the laser radial profile radius of the core is $R_c = 0.6$ mm ($\frac{1}{2}$ of the BSA setting, 1.2 mm), the resultant σ_r is 0.46 mm compared to $\sigma_r = 0.31$ mm from analysis of the transverse distributions in Fig. 3 (see Appendix), indicating that the laser beam halo is significantly larger than the inferred from Fig. 3.

If both core and halo are not saturated ($Q_{th} \le Q_{max}$ and $\xi Q_{th} \le Q_{max}$), the total charge is $Q = Q_{core} + Q_{halo} = Q_{th}$. The model can be applied to the simultaneous fit of the measured four curves (Fig. 4) by using six parameters: $Q_{\max}$ for the flattop temporal laser pulse, $Q_{\max}$ for the Gaussian temporal laser pulse, ξ, η, measured QE with 7.75 MW RF gun power and measured QE for 4 MW RF gun power. For the space charge limit the following formula is used: $Q_{max}\,(7.75\text{ MW}) = Q_{max}\,(4\text{ MW})\cdot\frac{E_{cath}(7.75\text{ MW})}{E_{cath}(4.00\text{ MW})}$ separately for the Gaussian and the flattop laser temporal profiles. In this formula, E_{cath} corresponds to the accelerating cathode field for each RF gun power setting at the moment of emission (see Eq. (1)), which is at the MMMG for each case. The results of the fit are shown in Fig. 4, and the fit parameters are summarized in Table 2.

Fig. 4 shows reasonable agreement of the semi-analytical model in the transition region between the SC and the QE limited emission regimes for the flattop cases, but quite poor agreement for the Gaussian cases. The results in Fig. 4 show that the measured charge versus laser energy curve for setup 1 is much stronger saturating than the yield of the modeling, whereas the opposite behavior is observed for setup 4. These discrepancies could be due to the dependence of the space charge density limit on the cathode accelerating field, which is assumed to be $\sigma_{scl} \propto E_0 \sin\varphi$. A more complicated dependence seems more adequate considering transient emission and image charge effects strongly dependent on the laser pulse temporal profile and the cathode accelerating field at the moment of emission. These considerations are studied with additional laser transverse distributions and bunch charge measurements compared to ASTRA simulations in the next subsection.

3.2. Numerical (ASTRA) simulations with core + halo particle distributions and comparison with experimental data

If the presumed homogeneous flattop transverse laser profile is used as input particle distribution in ASTRA with the measured rms size (red profile in Fig. 5), the bunch charge as a function of input charge (scaled to the laser pulse energy) saturates in the SC limited emission regime (red trace in Fig. 6). If an arbitrarily larger rms laser spot size is chosen for the ASTRA input particle distribution with flattop radial profile (orange distribution in Fig. 5), then the saturated charge level is higher (orange trace in Fig. 6) than that shown by the read trace in Fig. 6, but still does not match the experimental data trend (green circles in Fig. 6).

Taking into account the presence of halo based on our characterization of the laser transverse distribution, one can then create customized input particle distributions for the ASTRA simulations composed of a radially homogeneous core with a Gaussian-like decaying halo (see Eqs. (2) and (3)). A different MatLab script is utilized to create the new core + halo input particle distribution. The script takes an initially homogeneous radial distribution and scales the macro-particle charge

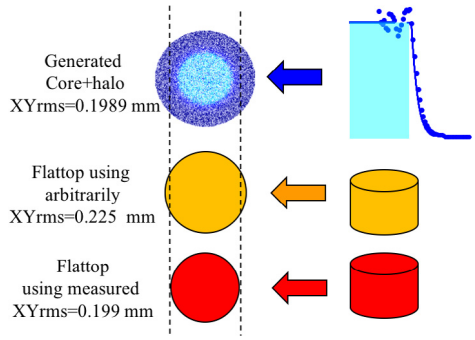

Fig. 5. Customized radial profile based on fitting parameters to the measured laser radial profile (top right), and resulting particle distribution with the macro-particle charge scale accordingly to Eq. (2) as shown by the post-processing ASTRA software. (For interpretation of the references to color in this figure legend, the reader is referred to the web version of this article.)

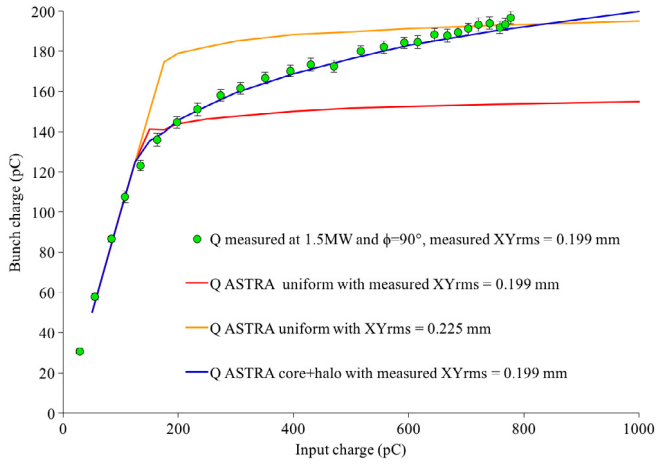

Fig. 6. Measured (green circles) and simulated (solid lines) charge Q as a function of input charge scaled to laser pulse energy for setup 5 in Table 1. Red trace: ASTRA simulation with homogeneous radial profile and XY rms set to measured value of 0.199 mm. Blue trace: ASTRA simulation with core + halo radial profile with fit parameters R_c = 0.34 mm, σ_r = 0.13 mm and resulting XY rms = 0.199 mm (identical to the measured value). Orange trace: ASTRA simulation with homogeneous radial profile XY rms arbitrarily set to a larger value than the measured. (For interpretation of the references to color in this figure legend, the reader is referred to the web version of this article.)

accordingly to $R_{mathrmc}$ and σ_r found from the fit parameters in Eq. (2) to the measured laser radial profile (Fig. A.2 in Appendix). When the generated core + halo input distribution is implemented in ASTRA (Fig. 5, top), the simulation results are in close agreement with extracted charge measurements as shown by the blue trace in Fig. 6, for which the simulated curves have the same set of laser and RF gun parameters for setup 5 (Table 1), with the exception of the shape of the radial profile.

3.3. Sensitivity of the core + halo model implemented in ASTRA to the radial profile fit parameters

For a given set of RF gun parameters, the behavior of the measured charge vs. input charge curves depends on the radial laser profile parameters R_c and σ_r that are utilized to generate the ASTRA core + halo input particle distributions. The fitting to find those parameters is influenced by several factors:

(a) Uncertainties in recording the laser transverse distribution captured by the UV CCD camera due to its sensitivity, dynamic range, background subtraction, etc. For example, if the laser beam intensity is low, the CDD might be insensitive to photons in the halo that fall below the detection threshold. If the laser intensity is high, the image of the core saturates yielding a larger diameter than the actual spot size on the photocathode, rendering an artificially larger halo than that determined with low laser intensities.

(b) Uncertainties in fitting R_c and σ_r to the obtained intensity radial profile, in particular as a function of laser intensity. Observations of radial profiles suggest that the amount of halo increases with laser pulse energy, but detailed measurements could not be performed due to camera saturation issues.

(c) Uncertainty in the measurements and estimations of the temporal profile of the photocathode laser pulse.

(d) Additional uncertainties are introduced by the laser system transport due to diffraction effects resulting in a ring-like structure of the laser transverse distribution at the cathode, plus potential inhomogeneities induced by the vacuum viewport and the vacuum mirror coupled to inhomogeneities in the cathode QE distribution.

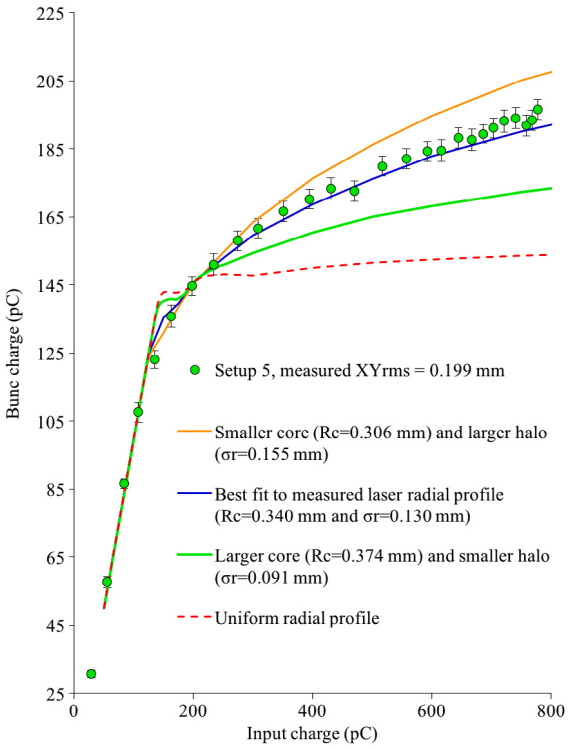

Fig. 7. ASTRA simulations using core + halo input distributions with indicated R_c and σ_r fit parameters adjusted in each case to maintain the rms spot size within 1% of the measured value, 0.199 mm corresponding to BSA = 0.8 mm in comparison with measured charge for setup 5 in Table 1. (For interpretation of the references to color in this figure legend, the reader is referred to the web version of this article.)

Figs. 7 and 8 illustrate the sensitivity of the core + halo model implemented in ASTRA to the radial profile fit parameters when the size of the core R_c is changed by 10% from the value that fits the measured radial profile (blue curves, Figs. 7 and 8), while σ_r is adjusted for each R_c value to maintain the rms spot size within 1% of the measured value (0.199 mm corresponding to BSA = 0.8 mm). If R_c is reduced, then σ_r needs to be increased resulting in more halo, and more halo means more charge in the SC limited emission region (see orange curves in Figs. 7 and 8). Notice that in this case, the core + halo model fits the experimental data in the transition regime but not in the SC limited emission regime.

In contrast, increasing R_c requires smaller σ_r resulting in less halo, therefore less charge in the SC limited emission regime (see green curves in Figs. 7 and 8). In this case, the model does not fit the experimental

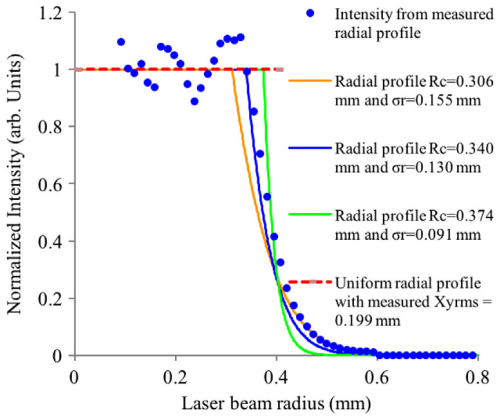

Fig. 8. Measured laser radial profile data for BSA = 0.8 mm in comparison with Eq. (2) for the R_c and σ_r fit parameters listed in Fig. 7. (For interpretation of the references to color in this figure legend, the reader is referred to the web version of this article.)

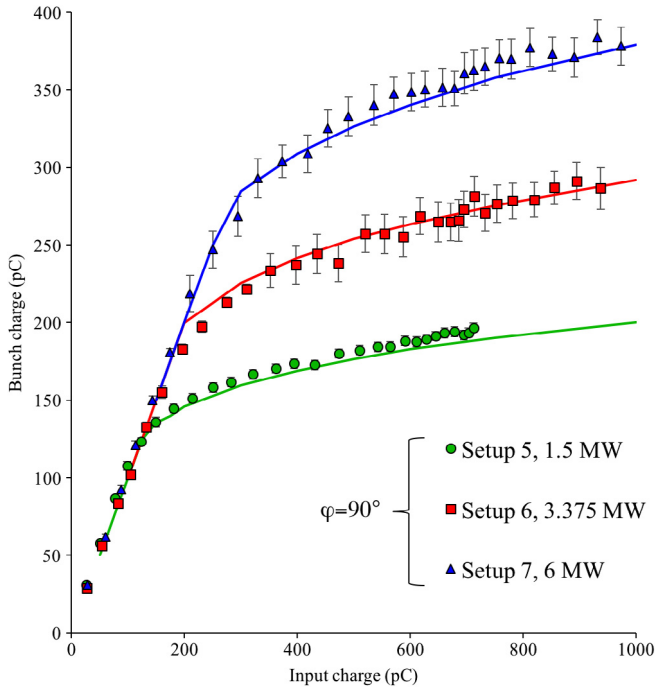

Fig. 9. Measured charge as a function of input charge scaled to laser pulse energy for setup 5–7 in Table 1. The solid curves show the corresponding ASTRA simulation results using the core + halo distributions with parameters R_c = 0.34 mm and σ_r = 0.13 mm that fit the laser rms spot size within 1% of its measured value, 0.199 mm corresponding to BSA = 0.8 mm.

data in the transition regime where the simulation shows the charge saturating before increasing again. The saturation behavior of the green curve in the transition regime is similar to the case with uniform radial profile, as shown by the dotted red curves in Figs. 7 and 8, indicating that the bunch charge saturates in the core before increasing again due to halo as the input charge increases

By utilizing the same generated core + halo distribution with R_c and σ_r that fit the measured radial profile, ASTRA simulations for setups 5–7 (see Table 1) agree well with the measured bunch charge as shown in Fig. 9.

To illustrate the uncertainty in the injector parameters, a series of experimental runs with 6 MW gun RF power were performed for BSA = 0.8 mm at 90, 49 and 30° RF gun phase (setups 8, 9, and 10 respectively in Table 1). The charge measured for each run is compared to the core + halo model implemented in ASTRA for those three phase values

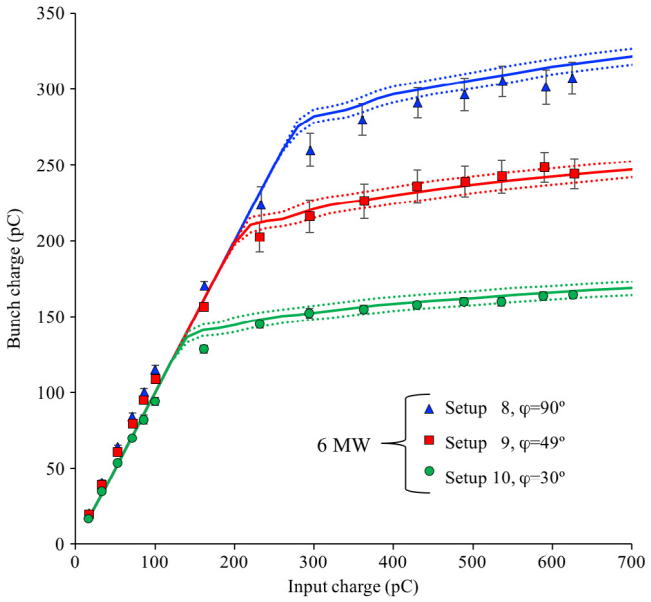

Fig. 10. Measured charge as a function of input charge scaled to laser pulse energy for setup 8–10 in Table 1. The solid curves correspond to the mean values from the core + halo model implemented in ASTRA with fitting parameters $R_c = 0.37$ *mm* and σ_r = 0.10 mm that fits the laser rms spot size within 1% of its measured value corresponding to BSA = 0.8 mm. The dashed curves are results of tolerance studies for the core + halo model applied. The error bars in Setup 8 (green disks) are smaller than the size of the marker. (For interpretation of the references to color in this figure legend, the reader is referred to the web version of this article.)

indicated by the solid curves in Fig. 10. The dashed curves show the sensitivity of the model when the phase is changed by ±1° from the mean value combined with "average ± rms" model (see Appendix) in the core + halo ASTRA simulations.

The transition between the QE and SC limited emission regimes seems to be the range where results of the core + halo model sometimes do not agree well with the experimental data. The discrepancy in the transition regime is not fully understood. For example, the ring structure present in the laser transverse distribution (see Appendix) was implemented into the core + halo model in ASTRA, but the agreement with the experimental data did not improve, while a less sharp transition was observed if the model was implemented using the average of the transverse distribution intensity ± the standard deviation around the azimuthal angle (the blue curve in Fig. A.2). It should be noted that the laser pulse used to obtain the curves in Fig. 10 was the shortest, ~2 ps as shown in setups 8–10 (Table 1), while the curves in Fig. 9 were obtained using 3.5 ps long laser pulses (setups 5–7 in Table 1). The only difference in setups 7 and 8 is therefore the duration of the laser pulse. The measured bunch charge for setup 7 in Fig. 9 is higher for a given input charge than that for setup 8 in Fig. 10. This observation indicates higher charge for longer pulses suggesting another signature of the transient character of the emission process, namely its dependence on the photocathode laser pulse temporal profile. In addition, the azimuthal inhomogeneity implemented in the model (blue curve in Fig. A.2) resulted in a smoother curve in the transition between the QE limited and the SC limited emission regimes. Explaining the remaining discrepancies requires full 3D simulations incorporating photoemission processes. Azimuthal inhomogeneity of the photocathode laser transverse distribution could imply local "hot spots" which could be saturated earlier than the overall integrated radial profile. This effect might be responsible for the remaining difference between measured and simulated emission dependences.

4. Conclusions

This work focused on studying the effect of unintended laser transverse halo on bunch charge from Cs_2Te photocathodes in an L-band

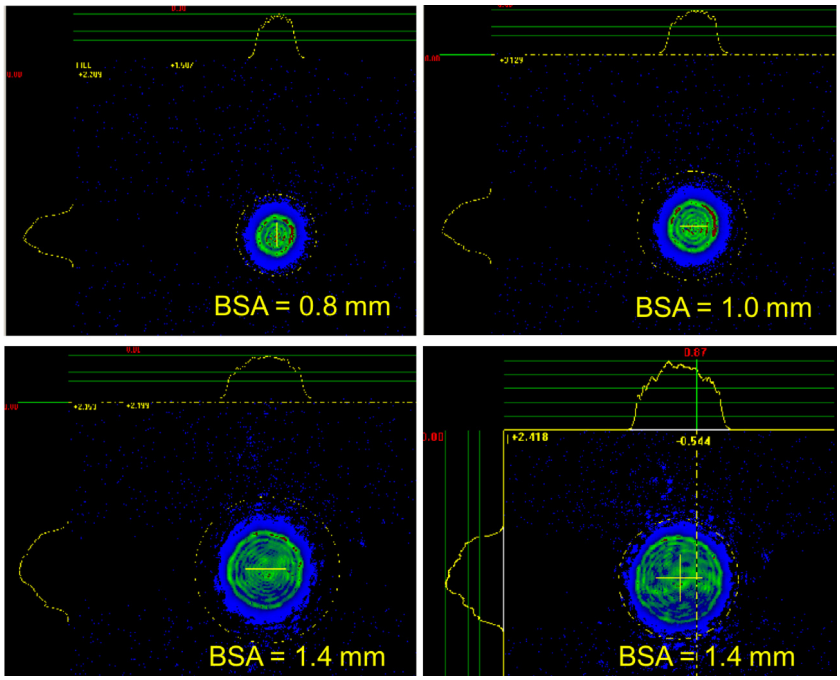

Fig. A.1. Pictures of the laser transverse distribution as captured by the CCD camera software for the indicated laser beam shaping aperture (BSA) settings. Projections from a circular region of interest are shown as well. The images were taken with background "envelope method" subtraction.

RF gun as a function of laser pulse energy for a wide range of laser spot transverse sizes, laser temporal pulse profiles, RF gun power and phase settings. Measurements consistently show the bunch charge increasing asymptotically in the space charge limited emission regime, while ASTRA simulations using a presumed ideal flattop transverse laser distribution show the expected bunch charge saturation.

In order to understand the source of this behavior, a semi-analytical emission model was applied to charge measurements for ~17 ps-long flattop and for ~2 ps-long Gaussian temporal laser pulses with similar laser radial profiles. The gun RF parameters were set to yield 29 and 45 MV/m accelerating cathode gradient at the moment of emission for each temporal profile. The semi-analytical model is based on a radially homogeneous core with Gaussian-like decaying halo derived from measurements of the laser transverse distribution illuminating the cathode. Although the model agrees reasonably well in the quantum efficiency limited emission regime (low laser pulse energy), the measured bunch charge saturates stronger than the model predictions for the short Gaussian pulse in the space charge limited emission regime (high laser pulse energy) with the cathode gradient set to 29 MV/m at the moment of emission, while the opposite is observed for the long flattop temporal laser pulses with the cathode gradient set to 45 MV/m at the moment of emission, even though both temporal profiles have very similar transverse distributions. These observations suggest that the asymptotic charge increase in the charge saturation region is induced by unintended halo present in the laser transverse distribution despite charge saturation in the core of the distribution, and that transient emission and image charge effects are strongly dependent on the cathode laser pulse temporal profile.

To test our hypothesis, custom particle input distributions composed of a flattop core with radius R_c and Gaussian-like decaying halo with σ_r were generated after fitting these parameters to radial profiles derived from the characterization of the laser transverse distributions illuminating the photocathode. When the core + halo customized input particle distributions are utilized, ASTRA simulations reproduce well the behavior of the measured bunch charge vs. laser pulse energy in the space charge limited emission regime for a wide range of laser spot sizes and RF gun parameters. In contrast, ASTRA simulations show expected charge saturation when only the presumed homogeneous flattop radial laser profile was used as input particle distribution.

However, the core + halo model implemented in ASTRA sometimes overestimates or underestimates the bunch charge measurements. The systematic limitations of this approach depend on the cumulative uncertainties related to the actual charge transverse distribution on the cathode, which in turn depends on the generated laser transverse distribution, the laser optical transport system and on the photocathode QE uniformity, on the measurement and characterization of the laser radial and temporal profiles (in particular for higher laser pulse energies where the CCD signal saturates), on the algorithm to derive an average laser radial profile, and on the manual fit of the core + halo parameters from the obtained radial profiles.

Despite these limitation, our analysis suggests that the unintentional presence of halo in the laser transverse distribution contributes to production of excess charge as the laser pulse energy increases in the space charge limited emission regime where the charge from the core has saturated.

Although the approach presented in this work attributes the observed charge behavior vs. laser pulse energy to the presence of halo in the cathode laser transverse distribution illuminating the photocathode, improvements of the laser transport system should minimize these effects, therefore rendering a distribution closer to the ideal homogeneous flattop radial profile.

Acknowledgments

The corresponding author would like to thank all colleagues from PITZ, specially to Dr. F. Stephan and Dr. M. Krasilnikov for the opportunity to work for one year at PITZ. Partial support for the corresponding author while on leave from Jefferson Lab provided by Jefferson Science Associates, LLC under US DOE Contract No. DE-AC05-06OR23177. The US Government retains a non-exclusive, paid-up, irrevocable, world-wide license to publish or reproduce this manuscript for US Government purposes.

Appendix. Treatment of the experimental laser transverse distributions

The transverse distribution of the photocathode laser is measured with a UV sensitive CCD camera (model JAE RM 1405, 12 bit) located

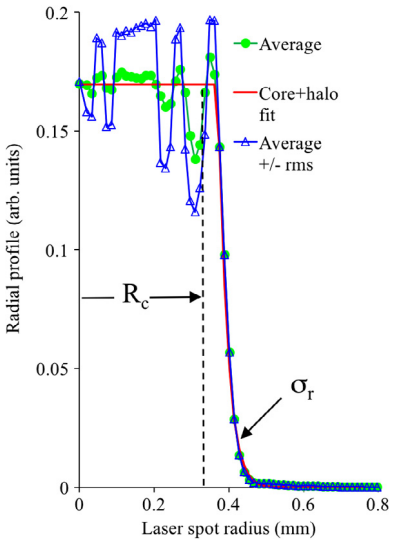

Fig. A.2. Illustration of the fitting parameters R_c and σ_r to the laser radial profile data according to Eq. (2). The core + halo radial profile corresponds to fit parameters $R_c = 0.34$ mm, $\sigma_r = 0.13$ mm and resulting XY rms = 0.199 mm (identical to the measured value) for BSA = 0.8 mm. (For interpretation of the references to color in this figure legend, the reader is referred to the web version of this article.)

at the position optically equivalent to the photocathode. By means of movable mirror the laser beam can be put onto the CCD chip of the camera (1040 × 1392 pixels). In order to use a full dynamic range of the 12-bit camera the laser intensity (if necessary the number of integrated laser pulses in a train) was adjusted. A typical procedure for image acquisition includes taking 20 frames with raw image and 20 frames of background while the laser shutter is closed. The background subtraction is performed using the "envelope" approach, in which each background pixel is assigned the maximum value found in all 20 frames for that particular pixel. This background image is subtracted from the laser beam image averaged over 20 frames. If the subtraction renders a negative value, then a value of zero is assigned to the pixel. In addition, the signal from each frame was analyzed separately, and then the results were averaged over the 20 frames. The difference between the frame-by-frame data compared to the averaged image fit is negligible, for the rms beam size the difference is less than 1%, for the core radius ~0.04%, and for rms halo width ~0.4%. Typical treated images of the laser are shown in Fig. A.1 for various laser spot diameters.

A procedure was developed to extract the laser radial profile from images like those shown in Fig. A.1, and also to quantify the amount of halo. A dedicated Matlab script reads the resulting image matrix, finds the center of mass in the matrix, makes a radial cut across the center and loads the values into a vector. A two-dimensional interpolation procedure is applied to find intensity value along a radial cut. The process is repeated over a series of azimuthal angles (typically, 36 divisions per quadrant for a total of 144 cuts) yielding a rotationally averaged radial profile—radial position and the averaged value of the intensity at each radial position. In order to reduce possible noise at the center of mass a small submatrix of pixels (typically ±5 pixels) is averaged. An example of the radial profile is shown in Fig. A.2 for the BSA = 0.8 mm. The obtained laser radial profile composed of a flattop core with Gaussian halo described in the main text by Eq. (2).

Each point of the radial profile could be supplied with an error bar calculated over all radial cuts. These (standard deviation) values reflect an azimuthal asymmetry of the laser distribution. In order to estimate an impact of the azimuthal density fluctuations onto the overall produced charge an additional radial profile (called "average ± rms", pink curve in Fig. A.2) is generated where the corresponding azimuthal density fluctuations are added to the average values (or subtracted from) if average values is larger (smaller) than the level of the flattop core (blue curve at Fig. A.2).

References

[1] F. Stephan, C.H. Boulware, M. Krasinlikov, J. Bahr, G. Asova, A. Donat, U. Gensch, H.J. Grabosch, M. Hanel, L. Hakobyan, H. Henschel, Y. Ivanisenko, L. Jachmann, S. Khodyachykh, M. Khojoyan, W. Köhler, S. Korepanov, G. Koss, A. Kretzschmann, H. Leich, H. Ludecke, A. Meissner, A. Oppelt, B. Petrosyan, M. Pohl, S. Riemann, S. Rimjaem, M. Sachwitz, B. Schoneich, T. Scholz, H. Schulze, J. Schultze, U. Schwendicke, A. Shapovalov, R. Spesyvtsev, L. Staykov, F. Tonisch, T. Walter, S. Weisse, R. Wenndorff, M. Winde, L.v. Vu, Detailed characterization of electron sources yielding first demonstration of European x-ray free electron laser beam quality, Phys. Rev. Spec. Top.: Accel. Beams 13 (2010) 020704.

[2] W. Ackerman, et al., Operation of a free-electron laser from the extreme ultraviolet to the water window, Nat. Photonics 1 (2007) 336–342.

[3] M. Altarelli, et al., DESY, Hamburg Report No. DESY 2006-097, 2007.

[4] S. Rimjaem, F. Stephan, M. Krasilnikov, W. Ackermann, G. Asova, J. Bahr, E. Gjonaj, H.J. Grabosch, L. Hakobyan, M. Hanel, Y. Ivanisenko, M. Khojoyan, G. Klemz, S. Lederer, M. Mahgoub, P. Michelato, L. Monaco, M. Nozdrin, B. O'Shea, M. Otevrel, B. Petrosyan, D. Richter, J. Rojsch-Schulenburg, D. Serotre, S. Schreiber, S. Schnepp, A. Shapovalov, R. Spesyvtsev, L. Staykov, G. Vashchenko, T. Wieland, I. Will, Optimizations of transverse projected emittance at the photo-injector test facility at desy, location zeuthen, Nucl. Instrum. Methods Phys. Res. A 671 (2012) 62–75.

[5] M. Krasilnikov, F. Stephan, G. Asova, H.-J. Grabosch, M. Gross, L. Hakobyan, I. Isaev, Y. Ivanisenko, L. Jachmann, M. Khojoyan, G. Klemz, W. Kohler, M. Mahgoub, D. Malyutin, M. Nozdrin, A. Oppelt, M. Otevrel, B. Petrysyan, S. Rimjaem, A. Shapovalov, G. Vashschenko, S. Weidinger, R. Wenndorff, Experimentally minimized beam emittance from an l-band photoinjector, Phys. Rev. Spec. Top. Accel. Beams 15 (2012) 100701.

[6] K. Flöttmann, ASTRA particle tracking code, available at http://www.desy.de/~mpyflo/.

[7] I. Will, G. Klemz, Generation of flat-top picosecond pulses by coherent pulse stacking in multicrystal birefringent filter, Opt. Express 16 (19) (2008) 14922.

[8] M. Gross, PITZ, private communication.

[9] J. Rosenzweig, N. Barov, S. Hartman, M. Hogan, S. Park, C. Pellegrini, G. Travish, R. Zhang, P. Davis, G. Hairapetian, C. Joshi, Initial measurements of the ucla rf photoinjector, Nucl. Instrum. Methods Phys. Res. A 341 (1994) 379–385.